Supplementary Materials to "An Opto-Thermocapillary Single Cell Manipulator"

1. Simulation of the Thermocapillary Flow Around the Bubble

In Fig. S1, the relationship between the bubble size and the lateral scale of the thermocapillary flow was simulated by finite-element modeling in COMSOL Multiphysics. The model geometry is shown in Fig. S1a. In Fig. S1b, the horizontal steady-state fluid velocities are plotted as a function of distance from the bubble center, measured along the white dashed line in Fig. S1a for three different bubble radii (5.0 μm, 2.5 μm, and 0.5 μm). The graph shows that the strength of the thermocapillary flow increases with bubble size, so a larger bubble has a wider horizontal influence. In Fig. S1c, similar horizontal fluid velocities for a hemispherical bubble with a 0.5-μm radius in water and 1% agarose solution are plotted. The increased viscosity of the agarose solution affects the thermocapillary flow velocity, making the range of horizontal flow smaller. The Marangoni numbers are 23.26, 5.81, and 0.23 for a bubble radius of 5.0 μm, 2.5 μm, and 0.5 μm, respectively in water (Fig. S1b), and it is 0.03 for a 0.5 μm-radius bubble in 1 % agarose (Fig. S1c) [1]. These results agree with that that reported by B. K. Larkins [2], in which smaller Marangoni numbers lead to a more localized thermocapillary convection.

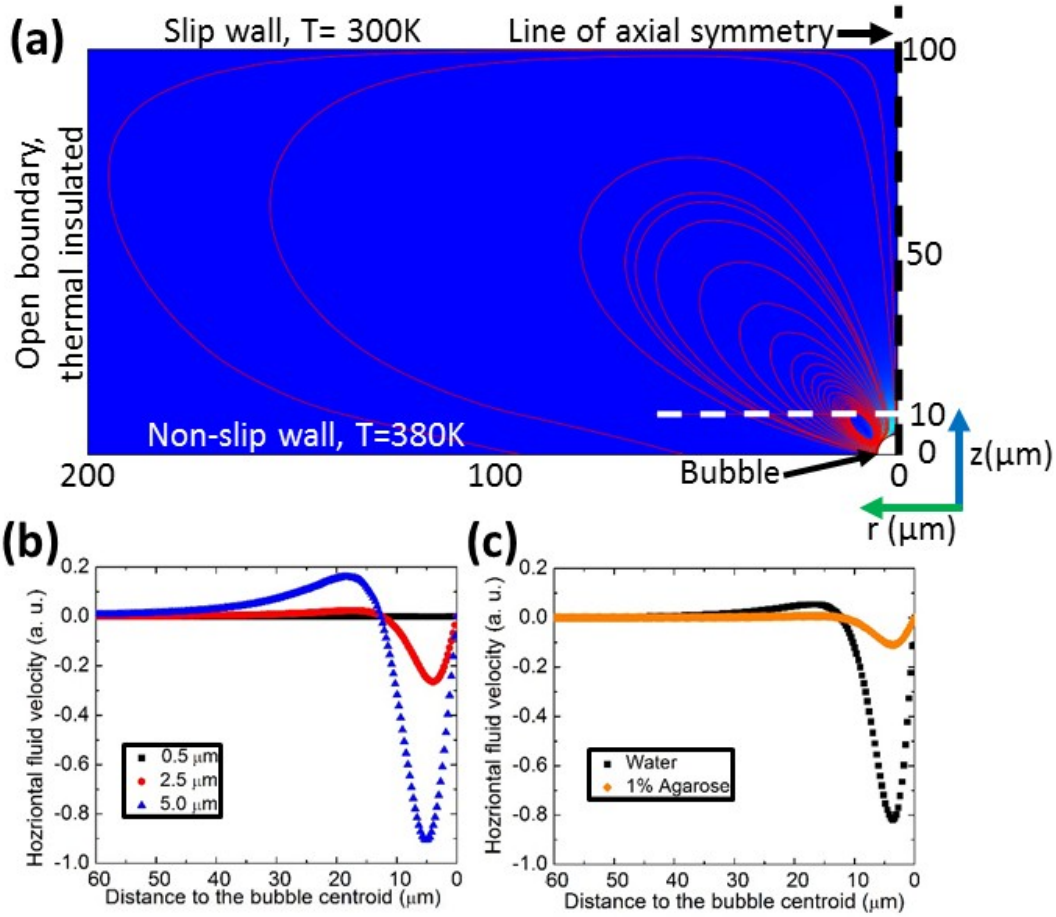

Fig. S1 (a) Simulation of the thermocapillary flow around a 5-μm-radius hemispherical bubble centred at the origin. (b) The horizontal fluid velocity as a function of distance from the centre of the bubble, measured along the white dashed line in (a) for different bubble sizes. The media simulated here is water. Positive velocities indicate fluid moving towards the origin. (c) The horizontal fluid velocity for a hemispherical bubble with a radius of 0.5 μm, in media with two different viscosities: water and a 1% agarose solution.

Property	Air	Water
ρ (Density)	1.161 kg·m^{-3}	0.997 kg·m^{-3}
η (Dynamic viscosity)	Not used	0.89 mPa·s
λ (Thermal conductivity)	0.026 W·m^{-1}·K^{-1}	0.607 W·m^{-1}·K^{-1}
Cp (Specific heat)	1007 J·kg^{-1}·K^{-1}	4181 J·kg^{-1}·K^{-1}

Table SI Properties of air and water at 25 ºC [3] used for the simulation shown in Fig. S2. Other parameters used include γ_T = 0.148 mN·m^{-1}·K^{-1} [4] and $\eta_{agarose}$ = 7 mPa·s [5].

In order to make a fair comparison of the flow velocities for different bubble sizes, each case must experience the same temperature gradient. Thus, for this simulation, the entire lower boundary is held at a constant temperature. (In the real OTMm, the temperature gradient is more realistically modeled as a Gaussian curve centered at the origin, but this would mean that bubbles of different sizes would have different temperature gradients at their surface.) Both conductive and convective heat transfer are considered outside the bubble. The fluid mechanics and convective heat transfer inside the bubble are ignored. The boundary condition on the bubble surface is set to:

$$\eta(\partial u/\partial \boldsymbol{n}) = \gamma_T(\partial T/\partial \boldsymbol{t})$$

where $\boldsymbol{n}$ and $\boldsymbol{t}$ are the unit vectors normal and tangential to the interface, respectively, η is the dynamic viscosity of water, u is the tangential component of the fluid velocity vector at the liquid/air interface, and T is the temperature [1]. The derivative of surface tension with respect to temperature is γ_T, and is given by $\gamma_T = \partial\gamma/\partial T$. The temperature is continuous across this boundary. The rest of the boundary conditions are indicated in Fig. S2a. The properties of the media are listed in Table SI.

2. Bubble Generation with Different Laser Pulse Widths

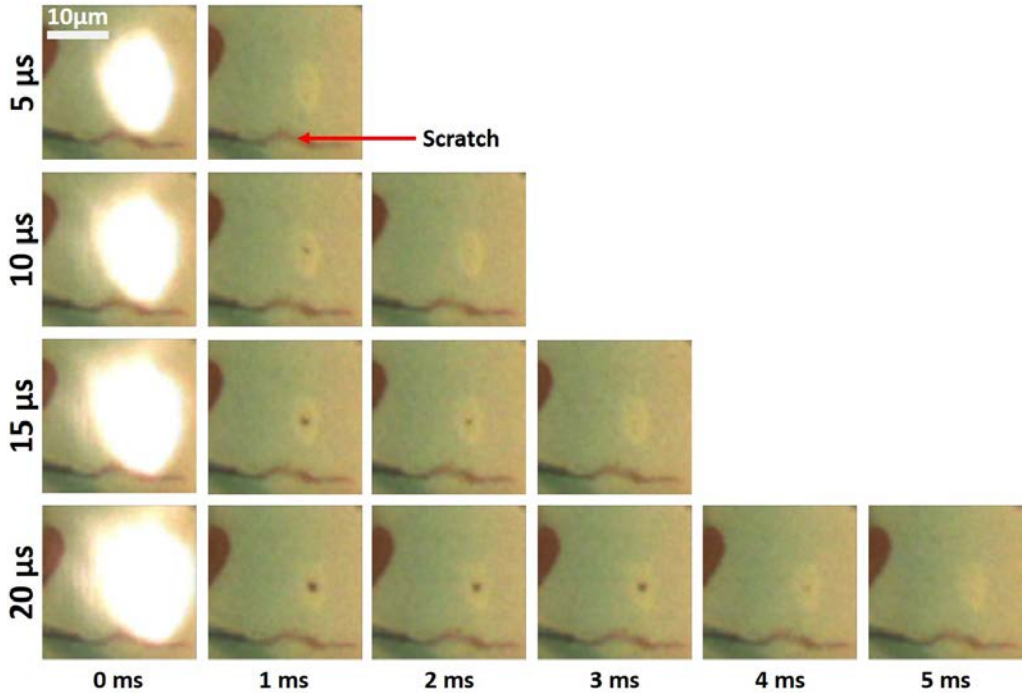

Fig. S2 Bubble generation with four different laser pulse widths. The bubbles were generated near a scratch on the surface of the ITO-coated glass. The video was recorded at 1000 frames per second.

The size of the generated bubble reduces with the decreasing pulse width (Fig. S2). The bubble diameters were about 1.5 μm, 1 μm, and 0.6 μm for pulse widths of 20 μs, 15 μs, and 10 μs, respectively. Smaller bubbles dissolved into the liquid more rapidly; bubbles disappeared within 5 ms, 3 ms, and 2 ms for pulse widths of 20 μs, 15 μs, and 10 μs, respectively. When the pulse width was 5 μs, the bubble dissolved too rapidly to be observed with the camera used to record these images. Since it only took less than 3 ms for a bubble generated by a 15-μs laser pulse to dissolve, and the shortest period between bubble generation events in current experiments was 10 ms (100 Hz), all the generated bubbles had enough time to dissolve before the next pulse.

3. Measurement of the *z*-Displacement of the Bead

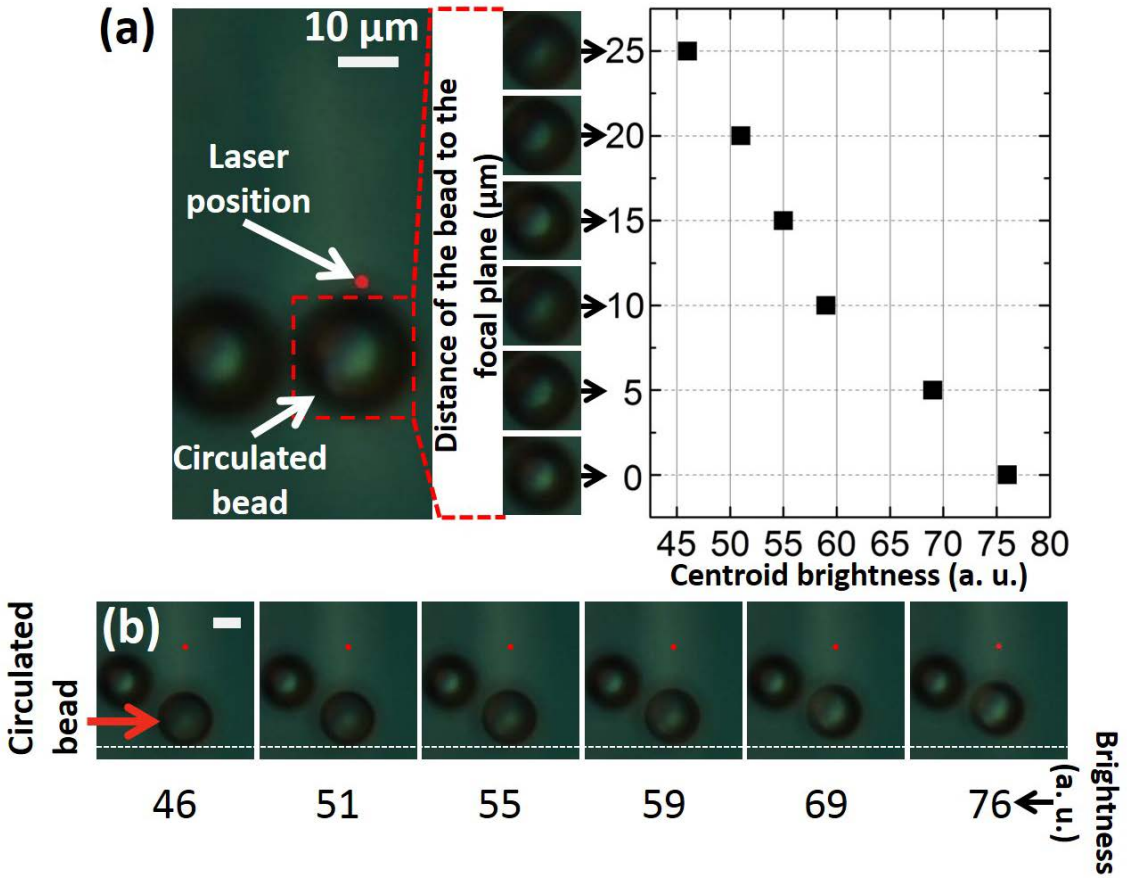

Fig. S3 Displacement in the *z*-direction correlated to bead centroid brightness. The laser pulse frequency is 20 Hz and the pulse width is 15 μs. The laser position is marked by a red dot. (a) Measurements of the reference bead centroid brightness when the laser is off. (b) *z*-displacements of the bead during circulation. The centroid brightness of the circulated bead is marked below each frame. The white dashed line is the reference line to detect the position of the beads. The scale bar is 10 μm.

Fig. S3 shows the method used to determine the *z*-direction displacement of microbeads in the OTMm. While the laser was off, the centroid brightness for the bead in Fig. S3a was recorded for different *z*-direction displacements, achieved by adjusting the specimen stage of the microscope using a Vernier micrometer (SM-25, Newport). The brightness of the image at the center of the bead was extracted using ImageJ software, and correlated to the *z*-direction displacement.

Once the bead brightness was correlated to *z*-position, the OTMm was used to create

thermocapillary flow, moving the bead. Fig. S3b shows a bead as it circulated back to the substrate surface. The circulating bead had an obvious *z*-displacement change (corresponding to a centroid brightness change) and a lateral displacement during this process. In comparison, the other bead has almost zero motion, due to stiction to the surface.

There is an artifact in this measurement method, since the emitting surface of the laser diode is reflective. This made the background of the region near the laser spot brighter, as shown in Fig. 5b of the main text. Thus, a bead would appear to be brighter when closer to the laser spot, and darker when it was away from the laser. This causes the evaluation of the *z*-displacement of the bead far away from the laser spot (25~30 μm) to be measured as larger than the actual value. This is the reason for the spike in the *z*-displacement of the microbead as it circulates away from the laser, as shown in Fig. 2a. There is no similar artifact when the bead is close to the laser spot, as this corresponds to the position of the bead during the initial correlation between bead brightness and *z*-displacement.

4. Probing the Temperature Distribution Around the Bubble

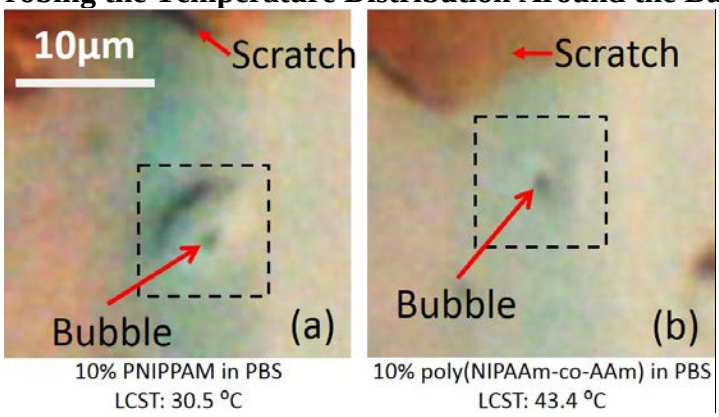

Fig. S4 Detection of the temperature profile in the OTMm by (a) 10% w/v PNIPAAm in PBS, and (b) 10% w/v poly(NIPAAm-co-AAm) in PBS. The laser was set to a pulse width of 15 μs at 100 Hz, and positioned near a scratch on the substrate. The video was recorded at 1000 frames per second.

Solutions of 10% w/v PNIPAAm (Mw: 19,000-30,000) in PBS and 10% poly(NIPAAm-co-AAm) (Mw: 20,000-25,000, Sigma Aldrich) in PBS were used to probe the temperature distribution around the laser-induced bubble. The laser pulse frequency was set to 100 Hz and the pulse width was 15 μs, representing the harshest conditions that the cells experience in the OTMm. The lower critical solution temperatures (LCST) of each solution were verified by a thermocouple (Type T probe, Omega HH806AU). The PNIPAAm solution had an LCST of 30.5 ºC, and the poly(NIPAAm-co-AAm) solution had a higher LCST of 43.5 ºC. Gelation of each solution occurs if the temperature is greater than the LCST. Figure S4 shows the gelation of PNIPAAm (Fig. S4a) and poly(NIPAAm-co-AAm) (Fig. S4b) immediately after a laser pulse. The radii of the gelled areas are about 3.5 μm and 2 μm, respectively. This indicates that the temperature was less than 43.4 ºC at a distance of 2 μm from the centre of the laser spot, and less than 30.5 ºC, which is safe for cells, at a distance of 3.5 μm from the centre of the laser spot.

However, there are limitations to the polymer-based temperature probing performed here that may lead to an overestimation of the temperature distribution around the bubble. First, the gelation of the temperature-sensitive polymers in Fig. S4 greatly reduces the convective heat transfer around the bubble, contributing to a temperature increase around the bubble. Secondly, even if the effects of the gelation were ignored, since both temperature-sensitive polymer solutions used here are more viscous than water, the temperature distribution result should not be

combined with the characterization results measured in water (Fig. 3a of the main text) to evaluate the temperature impact on the 20-μm-diameter bead. Thus, during cell manipulation, for those experiments in media with viscosity similar to water, such as PBS or DMEM, cells were circulated like in Fig. 3a, but the radius of the region with harmful temperatures is narrower than that in Fig. S4, due to the smaller viscosity of the water. On the other hand, for cell experiments in more viscous media such as PEGDA or agarose pre-polymer, the radius of the region with harmful temperatures is closer to that in Fig. S4. However, at the same time, the increased media viscosity reduces the strength of the thermocapillary flow, as discussed in Fig. S1, so the cells are not pulled to such a close distance to the laser-generated bubble as compared to the situation shown in Fig. 3a of the main text. Moreover, it should be noted that when the object is moving close to the bubble, its perpendicular velocity V_z increases sharply (Fig. 3b in the main text), reducing the negative impact of temperature on the cell.

5. Viability Tests on Cells Under Manipulation

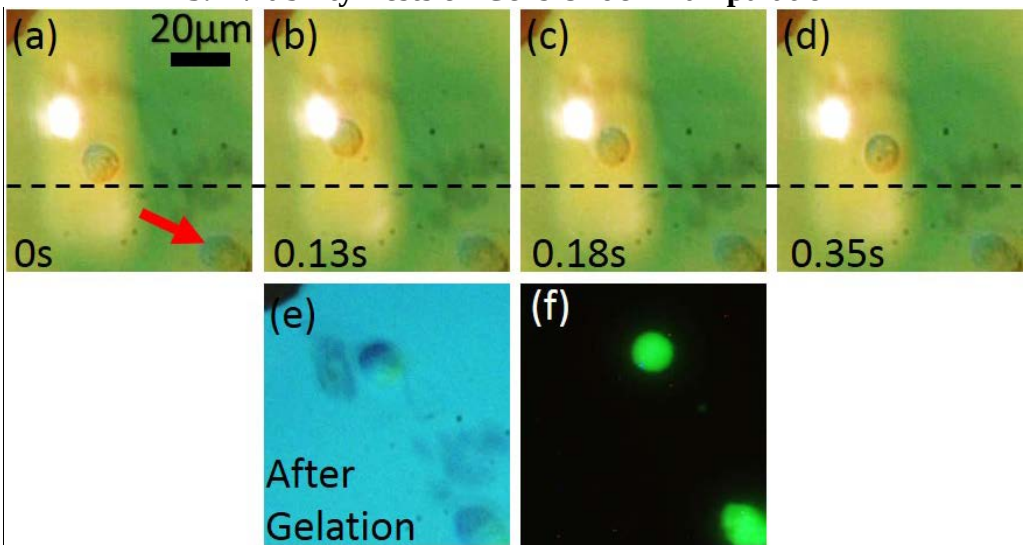

Fig. S5 (a-d) An NIH/3T3 cell circulating around a bubble. The red arrow marks a nearby cell as a point of reference. The black dashed line is the reference line to detect the position of the cell. (e) An image taken after the cell had been circulated for at least 20 times, followed by PEGDA gelation. (f) Viability test of the same cells in (a-e). Green fluorescence indicates that the cell is viable.

Fig. S5 shows a NIH/3T3 cell as it circulated around a bubble. The cells were in a 5% PEGDA pre-polymer mixture, prepared as described for the experiment shown in the Fig. 5 of the main text. The laser pulse frequency and pulse width were also set to be the same as that in the experiment shown in Fig. S4 (100 Hz, 15 μs). After the cell was circulated around the bubble at least 20 times, it was fixed on the substrate by gelling the PEGDA. The viability test was performed immediately after the PEGDA gelation, and indicated that the cell was still alive. The same test was repeated on 108 cells in total. Of these, 106 cells were observed to be viable, corresponding to viability of over 98%. The two negative cases may due to the selection of cells that were already dead.

6. Modified Device for Use with Agarose Solutions

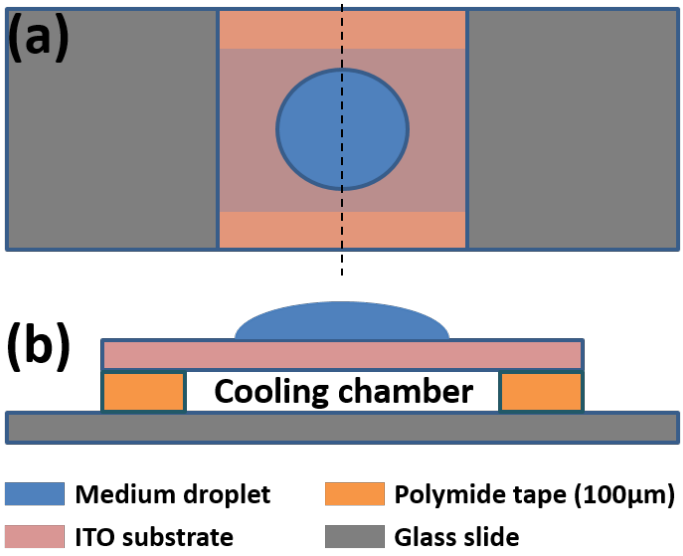

Fig. S6 The setup of the OTMm used when patterning cells in agarose. (a) Top view. (b) Cross section along the black dashed line in (a).

Fig. S6 shows the device used for cell manipulation inside agarose pre-polymer solutions. Laser absorption in the lower glass slide was found to be negligible. After the cell manipulation was completed, an ice cube was placed on one side of the cooling chamber. The icy water melt from the ice cube filled the cooling chamber due to capillary force. Filter paper was placed at the other side of the cooling chamber to absorb the icy water. This method creates a continuous flow of icy water through the cooling chamber, which drops the surface temperature of the ITO substrate to 11 ºC, with an ambient room temperature of 22 ºC. The lower temperature causes the agarose to gel.

7. Cell Migration Under Agarose Hydrogel

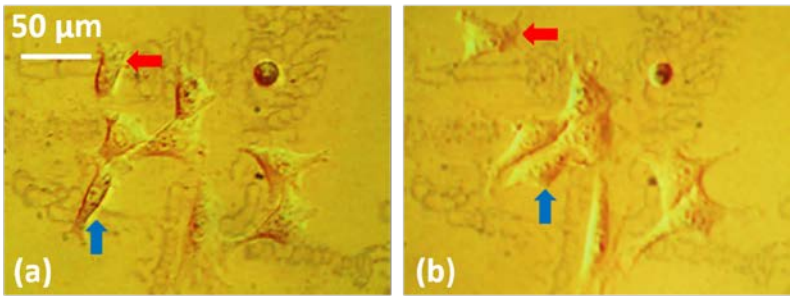

Fig. S7 Cell migration in agarose after (a) one hour and (b) two hours of culturing. The cells marked by the red and blue arrows have moved significantly. Note that (a) is the same as the Fig.6f in the main text.

Fig. S7 shows cell migration below agarose. Red and blue arrows mark the two cells with significant migration.

References

1. S. M. O'Shaughnessy and A. J. Robinson, *Annals of the New York Academy of Sciences*, 2009, **1161**, 304–320.

2. B. K. Larkin, *AIChE Journal*, 1970, **16**, 101–107.
3. W. M. Haynes, *CRC Handbook of Chemistry and Physics*, 92nd ed. CRC Press: Boca Raton, FL; 2011-2012.
4. R. S. Subramanian, R. Balasubramaniam, *The Motion of Bubbles and Drops in Reduced Gravity*, Cambridge University Press: Cambridge, UK, pp. 18.
5. D. R. Albrecht, G. H. Underhill, A. Mendelson, and S. N. Bhatia, *Lab on a Chip*, 2007, **7**, 702–709.